Eur. Phys. J. D **36**, 199–202 (2005)
DOI: 10.1140/epjd/e2005-00262-x

THE EUROPEAN PHYSICAL JOURNAL D

# VUV-heating of plasma layers and their use as ultrafast switches

A. Krenz[a] and J. Meyer-ter-Vehn

Max-Planck-Institut für Quantenoptik, Hans-Kopfermann-Str. 1, 85748 Garching, Germany

Received 20 May 2005 / Received in final form 10 August 2005
Published online 27 September 2005 

**Abstract.** We report on new possibilities to generate solid-density plasma at extreme energy density by intense VUV beams. Here we consider 100 fs pulses of 30 eV photons focused to $10^{16}$ and $10^{18}$ W/cm$^2$. The temperature evolution in 50 nm thick aluminum foils is discussed on the basis of simulations, performed with the one-dimensional radiation hydrodynamics code MULTI-fs. For 30 eV photons, the foil is shown to switch from transmission to reflection mode on a femto-second time-scale; this is due to the rapid change of the plasma frequency during laser heating which may turn an initially transparent Al-foil into an opaque one. The switching-time depends on the intensity of the laser pulse. Also layered heating structures inside the foil are discussed which occur due to reflection at the rear surface.

**PACS.** 52.50.Jm Plasma production and heating by laser beams (laser-foil, laser-cluster, etc.) – 52.38.Dx Laser light absorption in plasmas (collisional, parametric, etc.) – 78.20.Ci Optical constants (including refractive index, complex dielectric constant, absorption, reflection and transmission coefficients, emissivity)

## 1 Introduction

The TESLA Test Facility (TTF2) is a free electron laser (FEL) providing photons in the VUV region between 20–200 eV. The final XFEL (X-ray Free Electron Laser) planned for the coming years will produce photon energies up to 12 keV [1]. Similar beams will become available at the LCLS facility of the Stanford Linear Accelerator Center [2]. The VUV photons correspond to frequencies in the region of the plasma frequency $\omega_P$ of solid-density plasmas. This is also the region of peak coupling between photons and solid-density matter. For lower photon energies ($\omega_L < \omega_P$), the electron density is overcritical, and the light cannot propagate. For higher photon energies ($\omega_L > \omega_P$), thin foils are transparent, and the photo-absorption cross-sections decrease. The maximum energy deposition in solids occurs just in this region, where $\omega_L \approx \omega_P$. Therefore the VUV beams of TTF2 can reach plasma states in the same parameter range as the final XFEL, be it in thinner target foils (typically 50–100 nm). The VUV-FEL beam can generate solid-density plasma covering the full temperature range relevant e.g. for inertial fusion applications [3]. The uniformity of the plasma layers is of central importance. They expand in a planar way, making accessible a large range of densities. We anticipate that pump-probe experiments for measuring material opacities and equation-of-state properties will become possible, covering temperatures of 1 eV–1 keV and densities in the range of $10^{-3} < \rho/\rho_0 < 1$.

[a] e-mail: Annika.Krenz@mpq.mpg.de

The outstanding feature of the experiments now coming up at DESY [1] and also at the Stanford Linear Accelerator [2] is the high brilliance of the VUV beams, which were not accessible before. Plasma generation with VUV beams has been discussed before [4–6]. Actual experimental results obtained with high-order harmonics at much lower intensities have been reported by Theobald et al. [7]. Results on isochoric heating of solids with 150 fs optical pulses has been published by Eidmann et al. [8].

## 2 Simulation tools

In the following, we present simulations showing the heating of 50 nm thick foils of solid Al by 30 eV VUV-FEL photons. The results are obtained with the code MULTI-fs, which is a one-dimensional (1D) multi-group radiation hydrodynamics code. It has been developed for laser-matter interaction of ultra-short (100 fs) pulses [9,10]. The code solves the Maxwell equations in a steep gradient plasma. So far, it accounts only for collisional absorption by free electrons within the Drude model. At low temperatures, the collisional frequency is adapted to the cold transmission values taken from the Berkely CXRO tables [11].

These hydrodynamic codes are based on the assumption of local thermal equilibrium (LTE), which may be in conflict with the 100 fs time-scale of the envisioned experiments. For solid-density matter, however, and temperatures in the range of 100 eV, electron-electron collision times are less than 1 fs and ion-ion collision times less than 10 fs so that electrons and ions are expected

to thermalize in their subsystems. On the other hand, electron-ion energy transfer typically occurs on a longer time-scale of about 100 fs [12]. The MULTI-fs code accounts for this by dealing with separate electron ($T_e$) and ion ($T_i$) temperatures. Corresponding tables for electron and ion equations of state as functions of mass density $\rho$ and temperatures $T_e$ and $T_i$, respectively, have been generated with the MPQeos code [13]. In the context of this paper, a crucial role is played by the average ionization $Z_i$, which determines the electron number density $n_e = Z_i n_i$ from the ion density $n_i$ and thereby plasma frequency, index of refraction, and VUV photon propagation inside the foil. This important quantity $Z_i(\rho, T_e)$ is also calculated in LTE approximation and is taken from the EOS tables.

Spatial energy transfer is treated by flux-limited electron heat conduction and multi-group radiation transfer, which also provides rough information about the self-emission spectra. Opacity coefficients have been calculated using the SNOP code [14,15]. For more precise diagnostics, spectroscopic resolution may be needed and requires post-processing of MULTI-fs output with more specialized codes. In the present simulations, the heat flux inhibition parameter is set to the free streaming limit ($f = 0.6$), suggested by solid-foil isochoric-heating experiments by Saemann [16], using visible light. One should notice that a couple of parameters used in these simulations have been adjusted to experiments with optical laser pulses and may need readjustment in the VUV regime.

Another limitation of the results shown below relates to the one-dimensional (1D) geometry of the present simulations, while the real beams have a transverse profile. In view of typical foil thicknesses much smaller than the focal diameter, full information can be obtained by folding the 1D results with actual transverse intensity profiles.

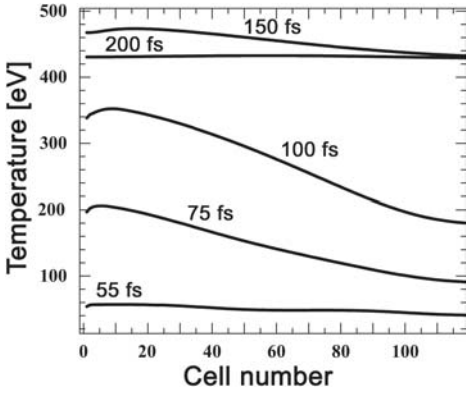


**Fig. 1.** Electron temperature distribution in an Al-target after 55 fs, 75 fs, 100 fs, 150 fs and 200 fs generated by a VUV beam with a photon energy of 30 eV (wavelength 41 nm), a FWHM pulse duration of 100 fs and an intensity of $10^{16}$ W/cm$^2$. The thickness of the foil is 50 nm. It is divided into 120 cells of equal mass. The laser pulse is incident from the left side.

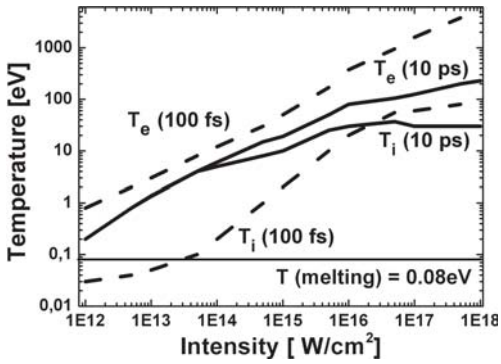


**Fig. 2.** Temperature as a function of pulse intensity for electrons and ions after 100 fs (dotted lines) and 10 ps (solid lines). The target is 50 nm thick, the pulse of 30 eV photons is 100 fs long.

## 3 Solid-density plasma

In Figure 1 and the following figures, a typical example is discussed relevant to the upcoming experiments at DESY. A VUV pulse of 30 eV photon energy and an intensity of $10^{16}$ W/cm$^2$ (alternatively $10^{18}$ W/cm$^2$) hits a solid aluminum target. A target thickness of 50 nm is chosen in this case, which is in the order of the absorption length of 30 eV photons in cold Al. For this thickness, a significant part of the incident pulse energy is absorbed in the layer, but also a sufficient number of photons is passing which is required for diagnostics purposes. The temporal development of the pulse is given by $\sin^2(\pi t/\tau)$, where $t$ is the time and $\tau$ is the FWHM pulse duration.

It is seen in Figure 1 that electron temperatures up to 450 eV are obtained for a peak intensity of $10^{16}$ W/cm$^2$. Corresponding pressures, not shown explicitly, range up to 500 Mbar. Hydrodynamic expansion is negligible during this short time period. At an intensity of $10^{18}$ W/cm$^2$, 5 keV temperature is obtained under these conditions. Such high electron temperatures can be reached, because the foil stays optically thin in this case and thermal radiation losses still do not dominate.

In Figure 1, it can also be seen that the high peak power VUV radiation deposits its energy rather uniformly in the volume initially, heating the thin foil isochorically such that the temperature is very uniform. After 75 fs up to 150 fs, a temperature gradient appears. This is because the heated foil then becomes overcritical (compare Sect. 4) such that absorption occurs predominantly near the irradiated surface. At 200 fs after the end of the heating pulse, the temperature profile equalizes again due to strong electron heat conduction. The maximum temperatures strongly depend on the intensity of the incoming VUV pulse. This is shown in Figure 2. The intensity on the target can be varied by changing the focus diameter. Physically, the temperatures depend on the laser absorption mechanism, the equation-of-state [13] and the partition of the absorbed energy into thermal and kinetic energy. Electron and ion temperature differ strongly at early times. This is because the beam first deposits its energy into electrons and the subsequent energy transfer to ions is slow due to the large mass difference.

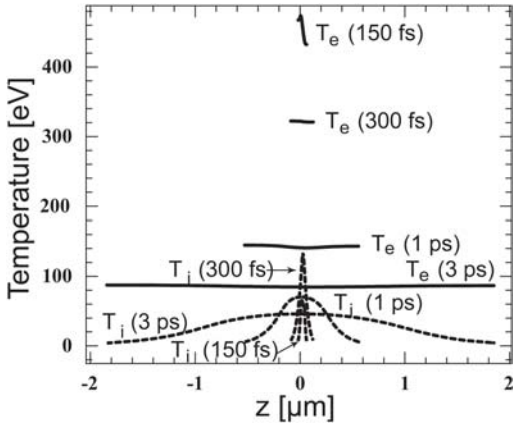


**Fig. 3.** Spatial evolution of electron and ion temperatures at 150 fs, 300 fs, 1 ps and 3 ps. The left surface of the original target is located at $z = 0$. Notice that the profiles are plotted versus real space coordinate to show foil expansion. These results refer to a 50 nm thick aluminum target irradiated by a $10^{16}$ W/cm$^2$ pulse of 30 eV photons with a FWHM pulse duration of 100 fs.

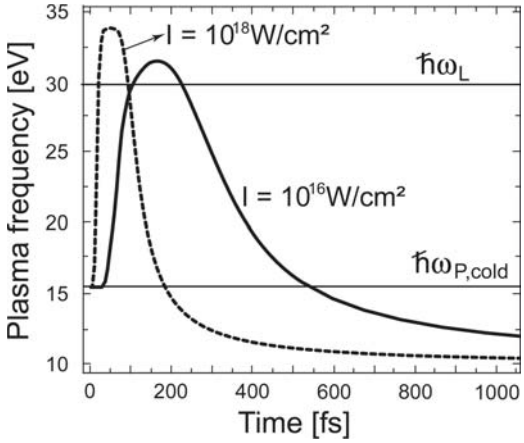


**Fig. 4.** Temporal development of the plasma frequency at an intensity of $10^{16}$ W/cm$^2$ and $10^{18}$ W/cm$^2$. The photon energy is 30 eV, the FWHM pulse duration is 100 fs, and the thickness of the Al-target is 50 nm; $\hbar\omega_{p,cold}$ denotes the plasma frequency of the cold Al target.

The temperature evolution during the hydrodynamic expansion stage after the end of the pulse is shown in Figure 3 for both electrons and ions at times 150 fs, 300 fs, 1 ps and 3 ps. Ion temperatures are seen to strongly lag behind for times shorter than 1 ps, but approach electron temperature for 3 ps. Rarefaction waves lowering the temperature are observed in the ion temperature curve at 1 ps on both sides of the foil, while electron temperature stays almost uniform also in the wings due to strong thermal conduction.

## 4 Target as a 10 fs switch

The irradiated foil can be used as a femtosecond switch. The switching occurs due to the fast change from the transmission to the reflection mode, when the plasma frequency $\omega_P$ rises from $\omega_P < \omega_L$ to $\omega_P > \omega_L$ during heating. This is illustrated in Figures 4–6; see also [12]. Since the plasma frequency depends on the density of free electrons in the plasma, $\omega_P \propto \sqrt{n_e} = \sqrt{Z_i n_i}$, it increases with rising ionization. This is shown in Figure 4. At an intensity of $10^{16}$ W/cm$^2$, the aluminum target is ionized up to $Al^{11+}$, and $\omega_P$ hits the photon frequency so that the pulse just cannot propagate anymore. In Figure 5 it is seen how this divides the 100 fs incident pulse into a 35 fs transmitted pulse and a 75 fs reflected pulse. All pulse durations refer to full width at half maximum (FWHM).

Raising the intensity to $10^{18}$ W/cm$^2$, also K-shell electrons are ionized and the plasmon energy $\hbar\omega_P$ rises to 33 eV. In this case, heating occurs much faster. Transmission is cut off already at 15 fs, and the switching time amounts to 7 fs only. This is seen in Figure 6. While transmission drops from nearly 88%, the value given in the Berkely CXRO table, to less than 10%, absorption and also reflection at the front surface of the foil are increasing. Of course, also hydrodynamic expansion is faster

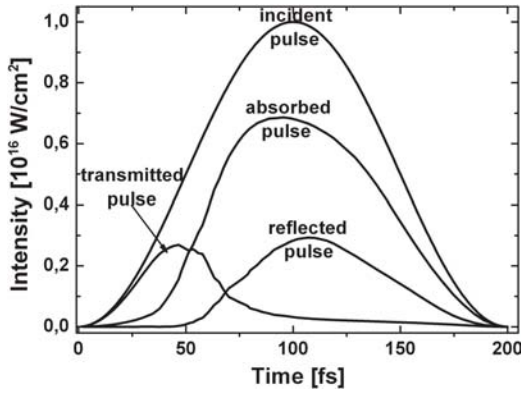


**Fig. 5.** Fragmentation of the incoming $\sin^2$-pulse into a reflected, a transmitted and into an absorbed pulse for an intensity of $10^{16}$ W/cm$^2$. Parameters same as in Figure 4.

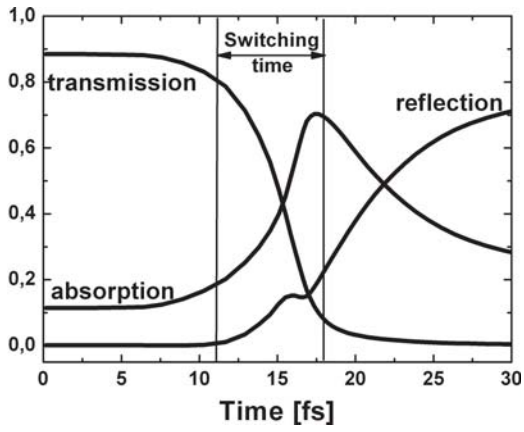


**Fig. 6.** Time dependence of the transmission, reflection and absorption of the pulse for an intensity of $10^{18}$ W/cm$^2$. The switching-time amounts only 7 fs. Parameters same as in Figure 4.

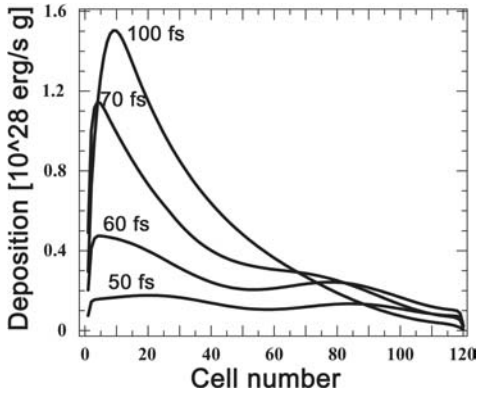


**Fig. 7.** Stratified energy deposition after 50 fs, 60 fs, 70 fs and 100 fs, for a photon energy of 30 eV and a FWHM pulse duration of 100 fs in a 50 nm thick aluminum foil. The foil is divided into 120 equal cells.

in this case because of much higher foil temperature and pressure. Therefore light transmission recovers already at about 115 fs, and, as a result, we have two transmitted pulses separated by a time interval of 100 fs. In actual experiments, time-dependent ring-like structures will appear, since the laser intensity has a transverse profile so that transmission and reflection depend on radius.

These are just illustrative examples. It is seen that the transition from transmission to absorption occurs very rapidly. The switching-time depends on intensity. If the intensity is higher, ionization occurs faster and therefore the plasma frequency reaches the photon frequency earlier. This allows in principle to slice the incident pulse into pieces with short rise times and large contrast ratios. These fast switching properties may be of interest in applications, where pulses much shorter than 100 fs with sharp rising edges are required. Another possibility is to use the foil as a plasma mirror for shaping VUV pulses with high contrast ratios.

## 5 Stratified energy deposition

Another surprising effect is observed in Figure 7. Inside the foil, the power of deposited laser energy reveals spatial oscillations for intermediate times. This phenomenon is related to inner reflection at the rear surface. It shows up for photon frequencies somewhat below, but close to the plasma frequency, where the plasma index of refraction tends to zero and reflection becomes strong. A standing wave then builds up inside the foil and leads to a layered deposition structure. In the peaks of this standing wave the laser deposition is higher, and so is ionization. The layered ionization structure further enhances the inner reflection. In this way, the standing wave self-amplifies until propagation is stopped because the plasma becomes overcritical; see curves for 100 fs and later. Then the laser deposition falls off again exponentially in the target.

## 6 Conclusions

The generation of solid-density plasma layers by intense VUV-FEL radiation has been discussed in terms of simulation results. When the laser frequency coincides with the plasma frequency, ultra-fast switching from transmission to reflection behavior occurs and can be used to slice 100 fs pulses into shorter pulses. The present results are intended to illustrate general behavior. For particular experiments, they need to be adjusted to the actual parameters.

This work was supported by the Commission of the European Community within the framework of the Association EURATOM – Max-Planck-Institut für Plasmaphysik.

## References

1. Th. Tschenscher, G. Materlik, *TESLA Technical Design Report, Part V, The X-Ray Free Electron Laser*, DESY, Hamburg, 2002; see also `http://www-hasylab.desy.de/facility/fel`
2. See the website `http://www-ssrl.slac.stanford.edu/LCLS/` for information on the LCLS facility
3. S. Atzeni, J. Meyer-ter-Vehn, *The Physics of Inertial Fusion* (Clarendon Press, Oxford, 2004)
4. R.W. Lee et al., J. Opt. Soc. Am. B **20**, 770 (2003)
5. S.J. Moon, K.B. Fournier, H. Scott, H.K. Chung, R.W. Lee, J. Quant. Spec. Rad. Transfer **81**, 311 (2003)
6. J. Meyer-ter-Vehn et al., Dense plasma physics studied with XFELs, in *Inertial Fusion Sciences and Applications 2003*, edited by B.A. Hammel et al. (American Nuclear Society, La Grange Park, Illinois, USA, 2004), p. 912ff
7. W. Theobald, R. Häßner, K. Kingham, R. Sauerbrey, R. Fehr, D.O. Gericke, M. Schlanges, W.D. Kraeft, K. Ishikawa, Phys. Rev. E **59**, 3544 (1999)
8. K. Eidmann et al., J. Quant. Spec. Rad. Trans. **65**, 173 (2000)
9. R. Ramis, R. Schmalz, J. Meyer-ter-Vehn, Comp. Phys. Commun. **49**, 475 (1988)
10. K. Eidmann, J. Meyer-ter-Vehn, T. Schlegel, S. Hüller, Phys. Rev. E **62**, 1202 (2000)
11. See website `http://www-cxro.lbl.gov`
12. A. Krenz, Diploma thesis, Technische Universität München, 2003
13. A. Kemp, *Das Zustandsgleichungs-Modell MPQEOS für heisse, dichte Materie*, Max-Planck-Institute for Quantum Optics, Report MPQ **229** (1998)
14. K. Eidmann, Laser Part. Beams **12**, 223 (1994)
15. G.D. Tsakiris, K. Eidmann, J. Quant. Spectrosc. Radiat. Transfer **38**, 353 (1987)
16. A. Saemann et al., Phys. Rev. Lett. **82**, 4843 (1999)